Published in final edited form as:
Lab Chip. 2009 February 21; 9(4): 545–554. doi:10.1039/b810571e.

A multipurpose microfluidic device designed to mimic microenvironment gradients and develop targeted cancer therapeutics

Colin L. Walsh, **Brett M. Babin**, **Rachel W. Kasinskas**, **Jean A. Foster**, **Marissa J. McGarry**, and **Neil S. Forbes**
Department of Chemical Engineering University of Massachusetts, Amherst Amherst, MA 01003-9303

Abstract

The heterogeneity of cellular microenvironments in tumors severely limits the efficacy of most cancer therapies. We have designed a microfluidic device that mimics the microenvironment gradients present in tumors that will enable the development of more effective cancer therapies. Tumor cell masses were formed within micron-scale chambers exposed to medium perfusion on one side to create linear nutrient gradients. The optical accessibility of the PDMS and glass device enables quantitative transmitted and fluorescence microscopy of all regions of the cell masses. Time-lapse microscopy was used to measure the growth rate and show that the device can be used for long-term efficacy studies. Fluorescence microscopy was used to demonstrate that the cell mass contained viable, apoptotic, and acidic regions similar to *in vivo* tumors. The diffusion coefficient of doxorubicin was accurately measured, and the accumulation of therapeutic bacteria was quantified. The device is simple to construct, and it can easily be reproduced to create an array of *in vitro* tumors. Because microenvironment gradients and penetration play critical roles controlling drug efficacy, we believe that this microfluidic device will be vital for understanding the behavior of common cancer drugs in solid tumors and designing novel intratumorally targeted therapeutics.

Keywords

microfluidic; tumor microenvironments; apoptosis; drug diffusion; pH

Introduction

The heterogeneity of cellular microenvironments in tumors severely limits the efficacy of most cancer therapies[1-4]. A microfluidic device that reproducibly mimics these microenvironments will enable the development of more effective cancer therapies. In tumors nutrient gradients create regions of cells that are necrotic, quiescent, or rapidly proliferating[5]. Most chemotherapeutics are only effective against proliferating cancer cells and have limited efficacy on quiescent cells[6, 7]. In addition, poor perfusion limits the ability of systemically administered drugs from penetrating interstitial tissue in sufficient concentrations to be effective[8, 9]. Controlling the delivery of therapeutics to all tumor sites is necessary to eradicate all cancer cells to prevent recursion and metastatic disease[10]. Development of therapies able to overcome this resistance to intratumoral delivery requires an *in vitro* device that can measure how molecules and treatment modalities localize and behave in three-dimensional tumor tissue.

Address correspondence to: Neil S. Forbes 159 Goessmann Laboratory Department of Chemical Engineering University of Massachusetts 686 North Pleasant Street Amherst, MA 01003-9303 Phone: (413) 577-0132 Fax: (413) 545-1647 forbes@ecs.umass.edu.

The geometric arrangement of blood vessels in tumor tissue is the major cause of microenvironment heterogeneity in tumors. The spatial arrangement of cancer cells in the vicinity of blood vessels is the key feature that must be emulated to create an effective tumor-mimicking device (Figure 1). Blood vessels in tumors non-uniformly deliver nutrients and remove wastes, which affects the distribution of cell types (Figure 1A)[11-14]. Close to the vessel wall, tumor tissue is well supplied with nutrients and rapidly proliferates. Further from the blood supply, the concentrations of nutrients decrease and cells become quiescent, apoptotic and eventually necrotic (Figure 1A)[5]. In addition, extracellular pH decreases with increasing distance from blood vessels[13].

Here we introduce the concept of a microenvironment gradient (Figure 1B) which is a continuous change in the chemical environment surrounding cells as a function of position. Microenvironment gradients form automatically in three-dimensional cells masses when the availability of nutrients is limited by diffusion[5]. The locations of different cellular regions parallel the concentrations of nutrients, growth factors and wastes, which are controlled by diffusion and consumption through successive layers of cells (Figure 1C)[14]. Changes in the microenvironment dramatically affect cell behavior; primarily causing growth arrest, apoptosis and cell death. Constraining a cell mass within a square box would force linear microenvironment gradients to form perpendicular to a nutrient source (Figure 1B). Linear microenvironment gradients would not mimic the complex radial and longitudinal gradients present in tumors[13, 15, 16], but would predictably reproduce the diversity of cell-types and environments surrounding blood vessels in tumors.

New therapeutic strategies are being designed to specifically target the quiescent, therapeutically resistant microenvironments that are unique to tumors and not present in normal tissue. These include nanoparticles[17, 18], viral particles for gene therapy[19, 20], and targeted bacteria[21, 22] (Figure 1A). In addition, acid-activated nanoparticles[23] and liposomes[24] have both been proposed as targeted cancer therapeutics. An *in vitro* device would be able to accurately quantify the penetration of novel therapeutics, measure their long-term effects on tissue viability, and assess their overall efficacy.

Two well-established methods of creating microenvironment gradients *in vitro* are tumor spheroids[5, 25] and sandwich cultures[26]. Spheroids are spherical clusters of cells grown suspended in culture medium. Nutrient diffusion through concentric cell layers creates the microenvironment gradients typically observed in human tumors *in vivo*[27, 28]. However, these gradients are difficult to study because the interior regions of spheroids cannot be observed microscopically and can only be investigated by physical cell dissociation[29]. Sandwich cultures create large millimeter-scale gradients by constraining monolayers of cells between glass slides[26]. Sandwich cultures enable the observation of cellular microenvironments using standard fluorescence microscopy[26], but do not capture the cell-cell interactions or interstitial diffusion resistances present in tumors.

Previous efforts to create micron-scale cellular bioreactors can be divided into two groups: those that contain monolayers and those that contain three-dimensional tissue. The design goal for most monolayer devices was to create a homogeneous environment without microenvironment gradients. A nanoliter bioreactor30 and a high aspect ratio device[31] have been designed to contain cell culture chambers molded in polydimethylsiloxane (PDMS) and microfluidic medium flow, in order to mimic the environment in cell culture flasks and microtiter plates. Micro-fabricated cell culture chips composed of polymethyl methacrylate (PMMA) with intergraded heat regulation and pH control have been shown to support cell growth for two weeks[32] and have similar gene expression to cells grown in culture flasks33. Mammary epithelial cells grown in microchannels constructed from enzymatically crosslinked gelatin exhibit morphological growth patterns similar to *in vivo* tumors[34]. PDMS microchannel

bioreactors have also been used to show that cells grow best with moderate medium flow and shear stress[35].

Polymer lithograph has been also used to culture three-dimensional tissues. Because it recreates cell-cell and cell-matrix interactions, three-dimensional culture has more closely related gene expression to *in vivo* tissue[36] and is more biologically relevant[37]. Recently, Lee and coworkers developed an elegant system to trap small spheroids in PDMS filter structures[38]. This system forms numerous 40 μm diameter spheroids with a narrow size distribution on a single microscope slide[38]. Similarly, Yu and coworkers have developed a system that utilizes microfabricated pillars and laminar flow complex coacervation to successfully grow cells for up to one week[37]. In addition to these designs, multiple bioreactors have been developed to engineer artificial tissues[39-43]. In these devices, the flow of nutrients by the surface was optimized to *reduce* gradients within the tissue[39, 41, 43]. None of these devices were created with the explicit purpose of reproducing microenvironment gradients.

We have designed a microfluidic device that mimics the microenvironment gradients present in tumors. The goals of the design process were to create a device that 1) enables simple introduction of cells, 2) creates predictable linear microenvironment gradients, 3) is easy to image microscopically, 4) is stable for long-term growth, and 5) can be used to test diffusion and localization of cancer therapies. The device was designed to mimic the tumor characteristics that reduce drug efficacy: a three-dimensional cell mass that limits molecular diffusion, low pH environments, and regions of therapeutically resistant cells. Multiple device designs were built and compared in order to achieve these design goals. Each tested design contained a micron-scale chamber exposed to medium perfusion on one side. All devices were made entirely of PDMS and glass to ensure optical accessibility and enable quantitative imaging of all regions of the cell mass. Fluorescence and time-lapse microscopy were used to demonstrate that the microenvironments in the device match those in *in vivo* tumors; measure long-term growth of the cell mass in the device; and quantify the penetration of multiple cancer therapies. Because microenvironment gradients and penetration play critical roles controlling drug efficacy, this microfluidic device will be vital for understanding the behavior of common cancer drugs in solid tumors and designing novel intratumorally targeted therapeutics.

Materials and Methods

Device Design and Construction

A series of devices were fabricated and tested to meet the design goals, make the device functional, and optimize its performance. All designs had a series of attributes in common. Each device consisted of a cell chamber, a flow channel, and connections to external tubing and a syringe pump to supply a constant flow of medium (Figure 2). In all designs the channel was greater than 5000 μm long, which is greater than three times the width of each tested cell chamber. This length was long enough to ensure well established laminar flow at the entrance to the cell chamber. A “spade” shape was used for the inlet and outlet ports to minimize volume and prevent cells from being trapped at the entrance to the channel.

Three variable design elements were modified by changing the photolithographic mask: 1) the chamber geometry, 2) the width of the flow channel, and 3) the geometry of the filter (Figure 2D-E). Seven different chamber geometries were created and tested (Figure 2D). Each had a unique width (from 350 to 1500 μm) and length, and tested three different aspect ratios (width to length; 1:1, 1:2 and 1:4). Two different channel widths were investigated: 125 and 250 μm (Figure 2D). Five different filter geometries were created and tested (Figure 2E). In all designs the total width of the filter was 250μm, the thickness of the posts was greater than 30μm, and the total area of open space (sum of the gap widths) was designed to be as large as possible.

As the number of posts increased, the thickness decreased. The aspect ratio of the posts (width to length) was 2:1 for each design.

PDMS layers containing imprints of the microfluidic devices were created using soft lithography[44]. Device designs were drawn using Illustrator (Adobe Systems Incorporated, San Jose, CA) and printed on high quality, 100 μm polyester-based Imagesetting film using an emulsion-based process (PageWorks, Cambridge, MA) to create micron-precision photolithographic masks. Negative images of the device features were made on photoresist-coated 100 mm silicon wafers (WaferWorld, West Palm Beach, FL). Wafers were coated with SU-8 2100 photoresist (Microchem, Newton MA) and spun at 1800 RPM to a thickness of 150 μm. Photoresist-coated wafers were covered with the lithographic masks and exposed to a 380 nm ultra-violet (UV) light source for 60 seconds to crosslink the photoresist. Non-crosslinked photoresist was removed by washing with SU-8 Developer (Microchem, Newton, MA) in a Pyrex dish under continual agitation. A final ethanol wash was performed to remove residual photoresist, and the wafer was allowed to air dry. A 2 mm thick PDMS (Sylgard 184, Dow Corning) layer containing an imprint of the design was cast by pouring a 10:1 mixture of monomer and curing agent over the photoresist relief. The PDMS was degassed for 20 minutes in a vacuum chamber to remove bubbles, cured for 2 hr at 60°C, and physically cut from the mold.

Completed microfluidic devices consisted of single PDMS layers adhered to a glass slide, nanoport connectors, external tubing, and a syringe pump (Figure 2B). Holes were drilled into the glass slides using ¾ mm diamond bits matching the locations of the inlet and outlet ports in the PDMS layer. The PDMS layer was adhered to the glass slide by subjecting both to oxygen plasma treatment at 200 mTorr for 7 minutes (Harrick Plasma Cleaner), assembling within 60 seconds of exposure, and heating overnight with applied pressure to improve adhesion. NanoPort connectors (Upchurch Scientific, Oak Harbor, WA) were attached to the glass slide directly above the holes in the slide using adhesive rings supplied by the manufacturer (Upchurch Scientific; Figure 2C). Adhesion of the connectors was enhanced by warming for 24 hrs. A flow system, consisting of inlet and outlet flows, was connected to the connectors to enable continuous medium delivery (Figure 2A-B). Cell packing required three ports and four flow streams: a packing inlet, a medium inlet, a packing outlet, and a medium outlet (Figure 2A-B). The packing inlet and the medium inlet were joined by a Y-valve prior to the inlet port (Figure 2A). A check valve (Upchurch Scientific) was added to the packing outlet stream to regulate the internal pressure of the device (Figure 2B).

Cell and Spheroid Culture

Human LS174T colon carcinoma cells were maintained in Dulbecco's Modified Eagles Medium (DMEM; Sigma Aldrich, St. Louis, MO) containing 10% fetal bovine serum (FBS) at 37°C and 5% CO_2. Tumor spheroids were formed by inoculating a single-cell suspension into culture flasks coated with poly(2-hydroxyethyl methacrylate), which prevented cell adhesion to the flask surface.

Cell Packing by Filter Retention

Introducing cells after the PDMS layer was adhered to the glass required that cells be “packed” into the chamber. Packing was achieved by flowing spheroids through the tubing and trapping them in a filter at the distal end of the chamber (Figure 2D-E). Prior to inserting cells, the assembled bioreactor was sterilized by flushing with 70% ethanol, followed by PBS to remove air and residual ethanol. A 10 mL syringe was filled with medium, connected to the inlet stream, and placed in a syringe pump (Harvard Apparatus; Figure 2A). Between five and ten spheroids were added to medium in a 1 mL syringe, which was connected to the packing inlet stream (Figure 2A). The medium outlet was crimped closed, and the cell solution was injected through

the reactor until a spheroid was trapped by the filter. Once the chamber was filled, the packing outlet was closed, the medium flow outlet was opened, and the syringe pump was started. A nominal flowrate of 3.0 μL/min produced an average linear velocity similar to that of blood in tumors (1.7 mm/sec)[45]. The entire device was maintained at 37°C in an enclosed environment that surrounded the microscope stage.

Spheroid Size

The effect of packing spheroids of different size was investigated by using different aged spheroids. We have previously shown that spheroid size can be controlled by varying the of growth time in culture[2]. The fill fraction was defined as the ratio of the area of the packed cell mass to the total area of the chamber. The area of the cell mass was determined from transmitted light images and visual inspection. Fill fractions represent averages of multiple measurements from each day. For each packing, the ability for spheroids to be retained by the filter and the quality of the cell mass was noted.

Long Term Growth

Tumor growth in the device was measured using time-lapse microscopy. A small spheroid was packed to fill approximately 50% of the chamber and allowed to grow. Medium was run through the device at 3 μL/min for 43 hours, and the device was incubated at 37 °C. Transmitted light images were taken at 0, 24, and 43 hours. The number of cells in the chamber was calculated by dividing the volume of packed tissue mass by the average cell volume, which was assumed to be 524 μm^3, based on a uniform 5 μm radius. The rate of growth was determined by linear regression.

Quantification of the Cellular Microenvironment

Diffusion of fluorescent dyes and drugs was quantified using an Olympus IX71 inverted microscope with a 10X Plan-APO fluorescence objective and IPLab imaging software (BD Biosciences, Rockville, MD). To create high-resolution images of the entire cell chamber, two 665.8 μm × 873.9 μm fields of view were tiled together using a specialized IPLab script. Time-lapse microscopy was performed by capturing images at regular intervals using an automated stage and image acquisition script. Microenvironment gradients were defined relative to the flow channel; the end of the chamber closest to the channel was designated “proximal” and the opposite end was designated “distal.” All staining used small-molecule dyes because antibodies-based stains do not diffuse sufficiently through tumor cell masses[2].

Cell viability was quantified using the Live/Dead Viability/Cytotoxicity Assay Kit (Invitrogen; Carlsbad, CA). This assay uses calcein AM and ethidium homodimer (Ethd-1) to identify viable and non-viable cells, respectively. Calcein AM fluoresces proportionally to intracellular esterase activity, and Ethd-1 binds to DNA in cells with permeable membranes. To simultaneously stain both viable and non-viable cells 1:2000 (v/v) calcein AM and 1:500 (v/v) Ethd-1 in DMEM were flowed through the device at 3.5 μL/min and 25 °C. Images were acquired 12 hours after packing the chamber and addition of the dyes.

The extent of apoptosis in the chamber was quantified using the CaspGLOW Red Caspase-3 Staining Kit (BioVision, Inc., Mountain View, CA). This assay uses DEVD-FMK conjugated to sulfo-rhodamine. DEVD-FMK is an inhibitor that irreversibly binds to activated caspase-3. The conjugated molecule (Red-DEVD-FMK) is a fluorescent marker that stains cells committed to programmed cell death. Apoptotic cells were identified by adding 1:1000 (v/v) Red-DEVD-FMK in DMEM to the 10 mL syringe and running the device at 3.5 μL/min and 25 °C. Images were acquired 17 hours after packing the chamber and adding the Red-DEVD-FMK dye.

Local cellular pH was quantified using 2',7'-bis-(2-carboxyethyl)-5-(and-6-)-carboxyfluorescein (BCECF) free acid fluorescent indicator (Invitrogen, Carlsbad, CA). Ratiometric measurement of BCECF fluorescence allowed concentration independent conversion from fluorescence to pH. Before staining, the device was packed and the cell mass was allowed to grow in the device at 37 °C with DMEM flowing at 3 μL/min for 24 hours. To stain for pH, 25 μM BCECF free acid in DMEM was run through the device at 3 μL/min at 37 °C. After 7 hours, fluorescent images at 440 and 495 nm were taken after washing the device and chamber with dye-free DMEM. The fluorescence ratio was adjusted for background fluorescence and converted to pH using the method described by James-Kracke[46]. The maximum and minimum values of the fluorescence ratio were determined by titrating BCECF in DMEM with NaOH and HCl, respectively46. This method produced identical results to the empirical method reported by Martin and Jain for pH measurement in tumors47.

Doxorubicin Diffusion

The rate of diffusion of doxorubicin (Dox), a common chemotherapeutic, was measured in the microfluidic device using time-lapse fluorescence imaging. The concentration of Dox was measured directly because it naturally fluoresces at 515 nm after excitation with 480 nm light[48]. Medium containing 10 μM Dox was delivered to the device at 3 μL/min for 32 hours at 25°C. Fluorescence images were taken every 30 minutes. The images were adjusted so that each time point displayed the same pixel value range and intensity values. Linear fluorescence intensity profiles were created by averaging the intensity of all pixels at a given linear distance from the front of the cell mass using a macro created in ImageJ (NIH Research Services Branch). Fluorescence intensity profiles were converted to concentration profiles by subtracting the background fluorescence and multiplying by the known concentration (10 μM) in the channel.

The effective diffusion coefficient (D) was calculated by modeling Dox transport through the system as simple Fickian diffusion through a semi-infinite solid.

$$\frac{\partial C_{Dox}}{\partial t} = D\frac{\partial^2 C_{Dox}}{\partial x^2} \tag{1}$$

Boundary conditions were established by assuming that initially (t=0) there was no Dox in the cell mass; the Dox concentration at the distal end of the chamber (x=∞) was zero; and the Dox concentration at the proximal end (x=0) equaled the concentration in the channel.

$$C_{Dox}|_{t=0} = 0$$
$$C_{Dox}|_{x=\infty} = 0 \quad C_{Dox}|_{x=0} = C_{Dox,channel} \tag{2}$$

Modeling diffusion using equation (1) assumes 1) that the concentrations in the channel are constant and well mixed; 2) that the cell mass is square, 3) that edge effects are minimal, and 4) that diffusion can be described with an effective diffusion coefficient. Least squares error analysis and the Solver function in *Excel* were used to fit the error function solution (Equation 3) to the concentration profile at 2, 4, 6, and 8 hours.

$$\frac{C_{Dox,channel} - C_{Dox}(x,t)}{C_{Dox,channel}} = erf\left(\frac{x}{2\sqrt{Dt}}\right) \tag{3}$$

To calculate the best-fitting diffusion coefficient for each concentration profile at a one time, the left side of Equation 3 was calculated at all positions. Then a diffusion coefficient was

guessed, the right side of Equation 3 was calculated, and the residue error between the two sides was determined. The guessed diffusion coefficient was adjusted to minimize the sum of the squares of all residues. An average diffusion coefficient was determined from the values calculated at each of the four time points.

Administration of Therapeutic Bacteria

The accumulation of fluorescently labeled therapeutic bacteria was measured as a function of time in the device. Bacteria were prepared as described previously[21, 22]. Briefly, a single colony of green-fluorescent-protein-expressing *Salmonella typhimurium* was suspended in LB with 250 mg/ml kanamycin and shaken for 4 hours at 37°C. This bacterial culture was centrifuged to remove the supernatant and re-suspended in cell culture medium (DMEM) with 250 μg/ml kanamycin to an estimated concentration of 1×10^6 CFU/ml. The device was packed and allowed to equilibrate for 8.5 hours at 37°C. Medium flow was kept at 3 μl/min throughout. An initial background image was acquired, and a syringe filled with the bacteria-containing medium was attached to the feed line. The medium syringe and pump were maintained at 4° C to limit bacterial growth. Transmitted and fluorescent pictures were taken at 28.5 hours, and a syringe containing medium without bacteria was attached to the feed line. At 45 hours final transmitted and fluorescent images were taken.

Results

Cell Insertion by Packing

Adhesion of the polymer layer to the glass surface prevented direct insertion of spheroids into the chamber of the device. To fill cells into the chamber, spheroids were inserted through the channels and trapped by a filter at the chamber's distal end (Figure 3A). Sealing the polymer layer to the glass slide created many advantages including, improved device sterilization, creation of well-defined borders for the cell mass, and prevention of leakage.

Five different filter geometries were designed to test the efficacy of increasing filter elements (see Methods). The optimum filter contained two elements (Figure 3A). Elements greater than 60 μm thick had uniform straight walls with minimal overhang or curvature (Figure 3C). As the number of elements increased, thickness decreased. All filter elements thinner than 60 μm broke during polymer casting or attachment to the glass. This occurred because thin filter elements were tall thin planes of material (150 × ~70 × ~35 μm) without structural rigidity in the vertical direction.

The addition of a check valve at the packing outlet (Figure 2B) improved the stability of cells within the chamber and increased the reliability of the packing process. Spheroids regularly washed out of devices fabricated without a check valve. Washout occurred at multiple times in the process: when the packing outlet stream was closed, when medium flow was initiated, and when the device was physically moved. Spheroids dislodged because the pressure in the packing outlet exceeded the pressure in the medium channel (Figure 2A). The addition of a check valve eliminated this back pressure, increased the overall stability of the system, and enabled the entire device to be physically moved. In addition, the check valve reduced the difficulty of the packing process because spheroids remained in the chamber once they were caught by the filter.

Device Geometry

Seven different chamber geometries were tested that modulated the width and length of the cell chamber (Figure 2D). The optimal aspect ratio was found to be 1:2. When the aspect ratio (width to length) was low (1:1), the chamber was not long enough and spheroids were washed out when medium flow was started. At the other extreme, when the aspect ratio was high (1:4),

the convective medium flow did not interact with the proximal edge of the tissue mass, which grew slowly, presumably because it did not receive sufficient nutrients. Within the tested range, small chambers (~350 μm wide) outperformed large chambers (500 – 1500 μm wide). Microenvironment gradients in both *in vitro* tissue and *in vivo* tumors are fully established in 100-150 μm^2, [27] (see Figure 5). Large cell masses contained a large proportion of necrotic tissue. Smaller masses were easier to form, more reproducible and more stable.

Two different channel widths were investigated: 125 and 250μm. The larger of the two widths (250μm) performed better because it reduced pressure gradients throughout the system. In addition, cell packing was more successful in devices with wider channels. During the packing process hand pressure was used to administer spheroid-containing medium. Devices with narrower channels had higher linear velocity and higher shear stress. As spheroids passed around the features of these devices the higher stress occasionally damaged and broke apart spheroids causing the packing process to fail.

The final device design consisted of a T-shaped system with a 350 × 700 × 150 μm (width × length × depth) cell chamber, 250μm channels, and three spade shaped inlet/outlet wells. A filter consisting of two posts, 65μm wide, 130μm long and with 40 μm gaps was located at the back of the chamber (Figure 2D-E). A cell-retention filter (Figure 3) and a check valve (Figure 2B) were used to trap tumor spheroids to fill the cell chamber (Figure 3B).

Spheroid Size

The extent that tumor tissue fills the chamber can be controlled by packing with different sized spheroids (Figure 4A-C). We have previously shown that spheroids grow with increased time in culture[2]. Spheroids less than or equal to 8 days old were too small to pack and flowed through the retention filter. Eleven day old spheroids successfully packed and filled approximately 25% of the chamber (Figure 4A-B). By 18 days, spheroids filled approximately 60% of the chamber (Figure 4A&C). After 21 days, spheroids became too large and fell apart during the packing process due to shear stress. The percentage chamber fill increased 3.2 ± 0.1% per day of spheroid growth in culture (Figure 4A). This dependence on age enables precise control of chamber fill for different experiments. For short term experiments (<24 hours), 16-18 day old spheroids that fill most of the chamber should be used. For long term experiments (>24 hours), 11-12 day old spheroids should be used to leave space for growth.

Long Term Growth

Tumor cell masses grew in the chamber at a linear rate of approximately 581 cells/hour, which corresponds to an increase in fill fraction of approximately 20% per day (Figure 4D). At this growth rate the device is capable of performing experiments lasting up to 96 hours if small 11-day-old spheroids are used to initially pack the device. For shorter experiments, the chamber can be initially packed to 80% and allowed to equilibrate and completely fill the chamber in 24 hours. A predictable and measurable rate of growth is also useful for drug studies because it provides a comparable baseline when measuring growth reduction and cell death.

Cellular Microenvironments

The primary design goal for the device was to create linear microenvironment gradients in *in vitro* tumor tissue. To test the ability of the device to produce these gradients, cell viability, the extent of apoptosis, and pH were measured as a function of position (Figure 5). As expected, cells were viable at the proximal end of the cell mass next to the medium flow and were dead at the distal end (Figure 5A). Cell death in cell masses was primarily caused by apoptosis (Figure 5B-C). Fluorescence in figures 5B-C indicates the presence of activated caspase-3, which is a downstream protease in the programmed cell-death pathway that indicates commitment to apoptosis. Caspase-3-dependent death has previously been observed in the

center of cylindroids[22]. Staining for cellular pH indicated that the environment was acidic in the interior of the cell masses and progressively more alkaline towards the exterior (Figure 5D). These microenvironment gradients are similar to those previously observed in cylindroids[2, 21], spheroids[5], and animal tumor models[12, 13].

The microenvironment gradients in the tumor masses developed after cells were packed into the device. This change indicates that the geometry of the chamber limited the availability of nutrients to predictably and controllably create proliferating and dead regions. The spheroids used to pack the device contained regions of viable cells and necrosis arranged in a radial pattern. If this pattern was maintained after packing, a region of viable cells would be visible along the edges of the tissue masses bordering the chamber walls (Figure 5A, indicated with arrows). However, the cells along the edge of the chamber were not viable; indicating the shape of the chamber and limited diffusion of nutrients rearranged the radial gradients creating a linear microenvironment pattern in less than 12 hours.

Chemotherapeutic Diffusion

The diffusion of doxorubicin in tumor masses in the device was quantified by acquiring a time-lapse series of fluorescence and bright field images (Figure 6A-B). The Dox concentration in the cell masses increased as a function of time and depth (Figure 6B). By fitting a diffusion model to linear fluorescence intensity profiles (Figure 6C) the diffusion coefficient was calculated to be 8.75×10^{-7} cm^2/s, which agrees with the previously reported value of 9.1×10^{-7} cm^2/s in human breast cancer[49]. The closeness of the fits shows that diffusion can be effectively modeled using the device. One limitation of this technique to measure diffusivity is that the drug molecule must be naturally fluorescent and adding a fluorescent tag may considerably affect the transport properties. This technique has an advantage over a standard technique, multicellular layer culture[50], because drug concentration can be measured continuously as a function of time and position.

Penetration of Anti-Cancer Bacteria

Long term accumulation patterns of *S. typhimurium* in tumor tissue were determined by delivering medium containing bacteria to the device for 45 hours. After twenty hours of flowing bacterial medium, fluorescent bacteria had penetrated to the distal end of chamber where they grew to concretions considerably greater than in the channel (Figure 6D). We have previously shown that wild-type Salmonella chemotax towards necrotic tumor tissue and preferentially grow there[21]. After flowing bacteria-free medium for 16.5 hours, the bacterial density continued to increase in the necrotic distal end of the cell masses (Figure 6E, arrow). The length of this experiment (45 hours) was longer than previous experiments using cylindroids (22 hours). In cylindroids long experiments were not feasible because of bacterial overgrowth[21], which did not occur in the flow device.

Discussion

These results show the utility of the designed microfluidic device as a platform to test novel cancer therapeutics. It successfully mimics the microenvironment gradients present in tumors (Figure 5) and can be used for long-term experiments (Figure 4). This is the first report of a device that creates linear gradients in physically constrained tissue bordering a channel of flowing medium. Because the design of the device is simple, it can be easily scaled to create an array of *in vitro* tumors for rapid drug development and tuning. The cell-retention filter at the rear of the chamber enables automated spheroid insertion for high-throughput robotic drug screening. Many therapeutics that have promise in monolayer cell screens are ineffective in solid tumors[51, 52]. A screening method that accurately mimics the cell-cell contacts and diffusion resistances in tumors (Figure 6B) is necessary to distinguish effective therapeutics.

The ability to model drug diffusion through a tumor (Figure 6) will enable prediction of drug concentrations at any position in the tumor at any time based on a drug concentration in the blood. This information can be used to determine appropriate dosages and predict the effectiveness of novel cancer therapies based on their ability to diffuse to different regions of a tumor. The potential to perform long-term experiments will enable drug delivery protocols that mimic physiological pharmacokinetics. In addition, the ability to observe and measure microenvironment changes in both time and space (Figure 5) will enable accurate predictions of drug efficacy. Many cancer drugs, e.g. paclitaxel, function by inducing apoptosis in tumors[53]. By comparing to an established baseline (Figure 5B), the extent that drug increases apoptosis and its location can be quantified.

A device that accurately mimics diffusion resistance in tumors will be necessary to develop therapeutics able to completely eliminate tumors and effectively treat cancer[1]. The device was able to characterize the transport differences between a passively diffusing therapeutic (doxorubicin) and actively penetrating vectors (Salmonella bacteria; Figure 6). When bacteria were added to the inlet medium, their ability to penetrate tissue and proliferate in distal regions was observed (Figure 6D-E). Previously, we have shown that salmonella can be genetically altered to control its tumor penetrating properties[1, 22]. We have also investigated modifying the surface properties of gold nanoparticles to control their penetrating properties[17, 18]. The ability to quantify diffusion resistance will be essential for developing and tuning these experimental tumor-penetrating therapeutics.

Conclusions

We have developed a device that contains three-dimensional tumor tissue exposed to continuously flowing media in order to mimic microenvironment gradients surrounding blood vessels in tumors. The optimum device design consisted of a 350 × 700 × 150 μm cell chamber, 250μm wide channels, a filter with two 65μm × 130μm posts and 40μm post-spacing. Eleven to 21 day old spheroids were inserted by packing, were shown to have long term viability, and could grow in the device for 96 hours. After insertion, the tissue microenvironment reproducibly rearranged, with viable cells next to the channel and apoptotic and necrotic cells deep into the chamber, and pH decreasing away from the medium supply. The device was able to accurately quantify the diffusion coefficient of doxorubicin, a common chemotherapeutic, and recreate the accumulation patterns of therapeutic *Salmonella*. This device is simple to construct, easy to image, and stable for long-term growth; it creates predictable microenvironment gradients and can be used to measure the diffusion and localization of any cancer therapeutic. This microfluidic device will be essential for tuning novel anti-cancer agents to overcome the microenvironment gradients and penetration limitations that limit the efficacy of current therapies.

Supplementary Material

Refer to Web version on PubMed Central for supplementary material.

Acknowledgments

We gratefully acknowledge financial support from the National Institutes of Health (Grant Nos. 1R21CA112335-01A and 1R01CA120825-01A1), the National Science Foundation (Grant No. DMI-0531171), and the Collaborative Biomedical Research Program at the University of Massachusetts, Amherst.

References

1. Forbes NS. Nature biotechnology 2006;24:1484–1485.

2. Kim BJ, Forbes NS. Biotechnology and bioengineering 2007;96:1167–1182. [PubMed: 17009333]

3. Jain RK. Nat Med 1998;4:655–657. [PubMed: 9623964]
4. Brown JM, Giaccia AJ. Cancer Res 1998;58:1408–1416. [PubMed: 9537241]
5. Sutherland RM. Science 1988;240:177–184. [PubMed: 2451290]
6. Jain RK. Annu Rev Biomed Eng 1999;1:241–263. [PubMed: 11701489]
7. Tannock IF. Cancer Metastasis Rev 2001;20:123–132. [PubMed: 11831640]
8. Tredan O, Galmarini CM, Patel K, Tannock IF. Journal of the National Cancer Institute 2007;99:1441–1454. [PubMed: 17895480]
9. Minchinton AI, Tannock IF. Nature reviews 2006;6:583–592.
10. Kim JJ, Tannock IF. Nature reviews 2005;5:516–525.
11. Vaupel P, Kallinowski F, Okunieff P. Cancer Res 1989;49:6449–6465. [PubMed: 2684393]
12. Helmlinger G, Sckell A, Dellian M, Forbes NS, Jain RK. Clin Cancer Res 2002;8:1284–1291. [PubMed: 11948144]
13. Helmlinger G, Yuan F, Dellian M, Jain RK. Nat Med 1997;3:177–182. [PubMed: 9018236]
14. Venkatasubramanian R, Henson MA, Forbes NS. J Theor Biol 2006;242:440–453. [PubMed: 16650438]
15. Dewhirst MW, Ong ET, Braun RD, Smith B, Klitzman B, Evans SM, Wilson D. Br. J. Cancer 1999;79:1717–1722. [PubMed: 10206282]
16. Erickson K, Braun RD, Yu D, Lanzen J, Wilson D, Brizel DM, Secomb TW, Biaglow JE, Dewhirst MW. Cancer Res 2003;63:4705–4712. [PubMed: 12907653]
17. Han G, You CC, Kim BJ, Turingan RS, Forbes NS, Martin CT, Rotello VM. Angew. Chem 2006;45:3165–3169. [PubMed: 16572498]
18. Hong R, Han G, Fernandez JM, Kim BJ, Forbes NS, Rotello VM. J. Am. Chem. Soc 2006;128:1078–1079. [PubMed: 16433515]
19. MacGill RS, Davis TA, Macko J, Mauceri HJ, Weichselbaum RR, King CR. Clinical & experimental metastasis 2007;24:521–531. [PubMed: 17653822]
20. Senzer N, Mani S, Rosemurgy A, Nemunaitis J, Cunningham C, Guha C, Bayol N, Gillen M, Chu K, Rasmussen C, Rasmussen H, Kufe D, Weichselbaum R, Hanna N. J Clin Oncol 2004;22:592–601. [PubMed: 14726502]
21. Kasinskas RW, Forbes NS. Biotechnology and bioengineering 2006;94:710–721. [PubMed: 16470601]
22. Kasinskas RW, Forbes NS. Cancer Res 2007;67:3201–3209. [PubMed: 17409428]
23. Shen Y, Tang H, Radosz M, Van Kirk E, Murdoch WJ. Methods Mol. Biol 2008;437:183–216. [PubMed: 18369970]
24. Karanth H, Murthy RS. J. Pharm. Pharmacol 2007;59:469–483. [PubMed: 17430630]
25. Sutherland RM, Durand RE. Recent Results Cancer Res 1984;95:24–49. [PubMed: 6396760]
26. Hlatky L, Alpen EL. Cell and tissue kinetics 1985;18:597–611. [PubMed: 4064103]
27. Freyer JP, Sutherland RM. Cancer Res 1986;46:3504–3512. [PubMed: 3708582]
28. Mueller-Klieser W. Critical reviews in oncology/hematology 2000;36:123–139. [PubMed: 11033302]
29. Freyer JP, Sutherland RM. Cancer Res 1980;40:3956–3965. [PubMed: 7471046]
30. Prokop A, Prokop Z, Schaffer D, Kozlov E, Wikswo J, Cliffel D, Baudenbacher F. Biomedical microdevices 2004;6:325–339. [PubMed: 15548879]
31. Hung PJ, Lee PJ, Sabounchi P, Aghdam N, Lin R, Lee LP. Lab on a chip 2005;5:44–48. [PubMed: 15616739]
32. Petronis S, Stangegaard M, Christensen CB, Dufva M. BioTechniques 2006;40:368–376. [PubMed: 16568825]
33. Stangegaard M, Petronis S, Jorgensen AM, Christensen CB, Dufva M. Lab on a chip 2006;6:1045–1051. [PubMed: 16874376]
34. Paguirigan A, Beebe DJ. Lab on a chip 2006;6:407–413. [PubMed: 16511624]
35. Korin N, Bransky A, Dinnar U, Levenberg S. Lab on a chip 2007;7:611–617. [PubMed: 17476380]

36. Zietarska M, Maugard CM, Filali-Mouhim A, Alam-Fahmy M, Tonin PN, Provencher DM, Mes-Masson AM. Molecular carcinogenesis 2007;46:872–885. [PubMed: 17455221]
37. Toh YC, Zhang C, Zhang J, Khong YM, Chang S, Samper VD, van Noort D, Hutmacher DW, Yu H. Lab on a chip 2007;7:302–309. [PubMed: 17330160]
38. Wu LY, Di Carlo D, Lee LP. Biomedical microdevices 2008;10:197–202. [PubMed: 17965938]
39. Fiegel HC, Havers J, Kneser U, Smith MK, Moeller T, Kluth D, Mooney DJ, Rogiers X, Kaufmann PM. Tissue engineering 2004;10:165–174. [PubMed: 15009942]
40. Braccini A, Wendt D, Jaquiery C, Jakob M, Heberer M, Kenins L, Wodnar-Filipowicz A, Quarto R, Martin I. Stem cells (Dayton, Ohio) 2005;23:1066–1072.
41. Cartmell SH, Porter BD, Garcia AJ, Guldberg RE. Tissue engineering 2003;9:1197–1203. [PubMed: 14670107]
42. Schmitmeier S, Langsch A, Jasmund I, Bader A. Biotechnology and bioengineering 2006;95:1198–1206. [PubMed: 16807928]
43. Navarro FA, Mizuno S, Huertas JC, Glowacki J, Orgill DP. Wound Repair Regen 2001;9:507–512. [PubMed: 11896993]
44. McDonald JC, Whitesides GM. Accounts of chemical research 2002;35:491–499. [PubMed: 12118988]
45. Forbes NS, Munn LL, Fukumura D, Jain RK. Cancer Res 2003;63:5188–5193. [PubMed: 14500342]
46. James-Kracke MR. Journal of cellular physiology 1992;151:596–603. [PubMed: 1295907]
47. Martin GR, Jain RK. Microvascular research 1993;46:216–230. [PubMed: 8246820]
48. Greupink R, Bakker HI, Bouma W, Reker-Smit C, Meijer DK, Beljaars L, Poelstra K. The Journal of pharmacology and experimental therapeutics 2006;317:514–521. [PubMed: 16439617]
49. Lankelma J, Fernandez Luque R, Dekker H, Schinkel W, Pinedo HM. Microvascular research 2000;59:149–161. [PubMed: 10625582]
50. Tannock IF, Lee CM, Tunggal JK, Cowan DS, Egorin MJ. Clin Cancer Res 2002;8:878–884. [PubMed: 11895922]
51. Olive KP, Tuveson DA. Clin Cancer Res 2006;12:5277–5287. [PubMed: 17000660]
52. Suggitt M, Bibby MC. Clin Cancer Res 2005;11:971–981. [PubMed: 15709162]
53. Weigel TL, Lotze MT, Kim PK, Amoscato AA, Luketich JD, Odoux C. The Journal of thoracic and cardiovascular surgery 2000;119:795–803. [PubMed: 10733772]

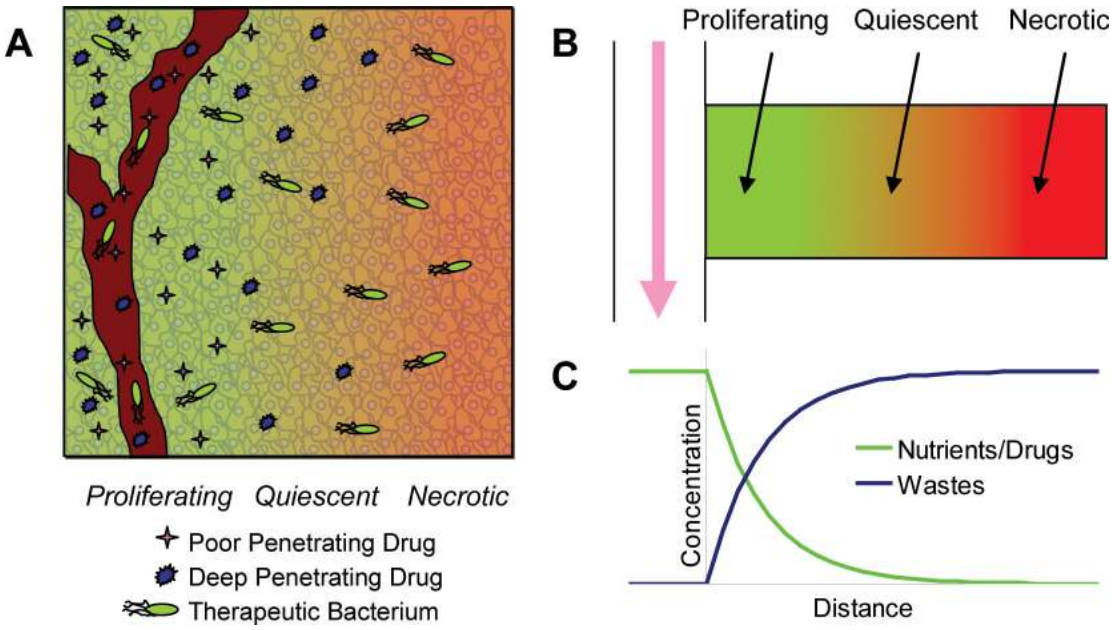

Figure 1. Microenvironments in the microfluidic device mimic those surrounding blood vessels in tumors

A) Nutrient and waste gradients away from vessels creates regions of proliferating (green), quiescent (transition), and necrotic (red) tissue. Drugs have varying penetration capabilities. Some penetrate deeply (blue stars), while others do not (purple crosses). Engineered bacteria (green ovals) have the potential to penetrate to therapeutically resistant regions. *B)* The linear, observable microenvironment gradients in the microfluidic device have a similar pattern to those surrounding blood vessels in tumors: proliferating (green), quiescent (yellow), and necrotic (red). *C)* Conceptual concentration profiles of nutrients (green), drugs (green), and wastes (blue) around blood vessels that are emulated by the device. Regions far from blood or culture medium are low in nutrients and drugs and high in wastes.

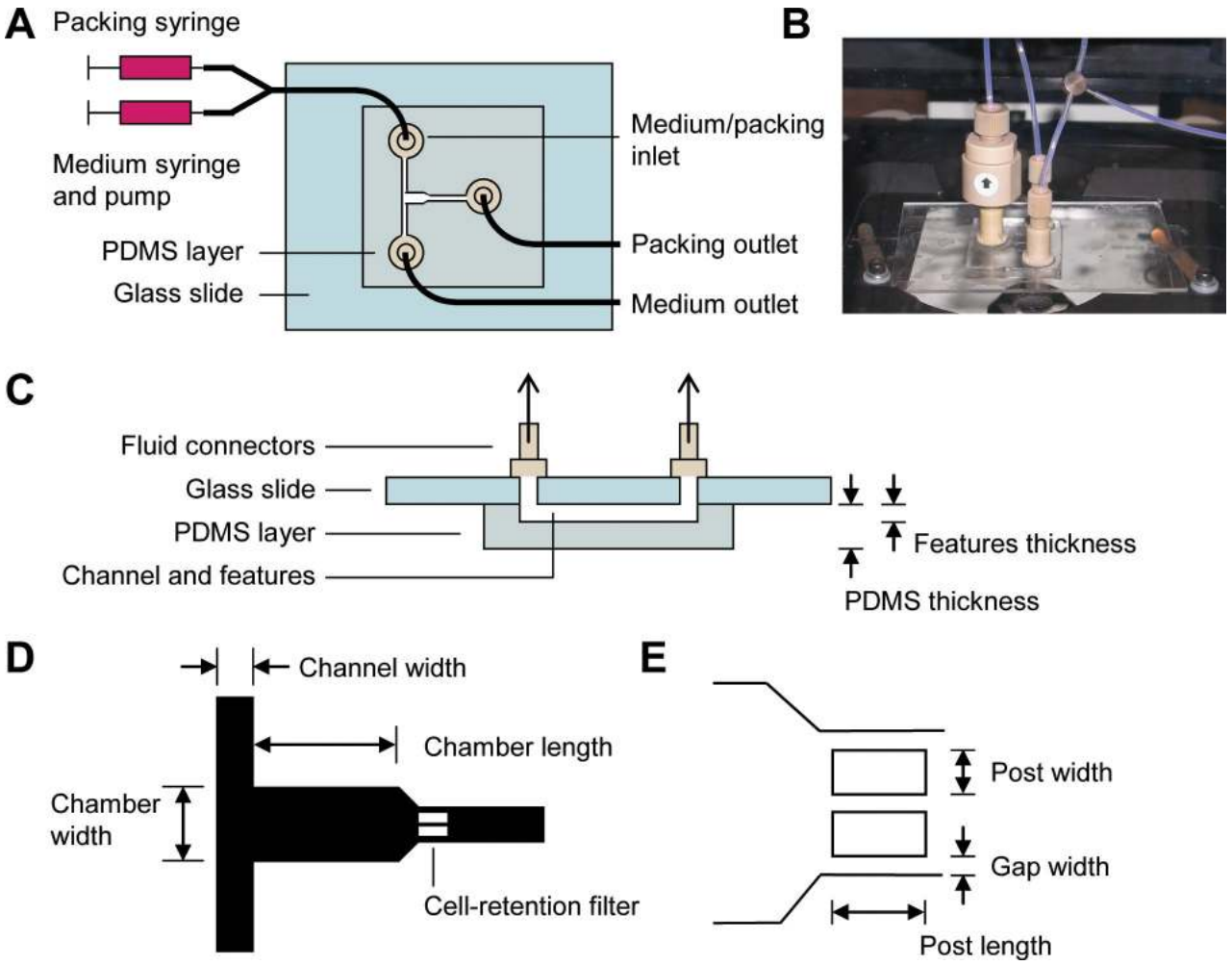

Figure 2. Design of the microfluidic tumor device

A) Top-view of the device showing the arrangement of the medium/cell inlet, the packing outlet, and the medium outlet. Both the spheroid-containing, packing syringe and the medium syringe were attached to the inlet. A check valve was attached to the packing outlet. *B)* Working device with flow inlets, outlets and check valve attached. *C)* Cross-section view of the device showing holes through the microscope slide used to connect to the fluid flow. *D)* Expanded image of the packing chamber in the center of the device in *(A)*. The adjusted dimensions of the chamber were width, depth, and channel width. The cell retention filter is shown at the distal end. *E)* Adjusted dimensions of the cell retention filter: post width, post length, and gap width.

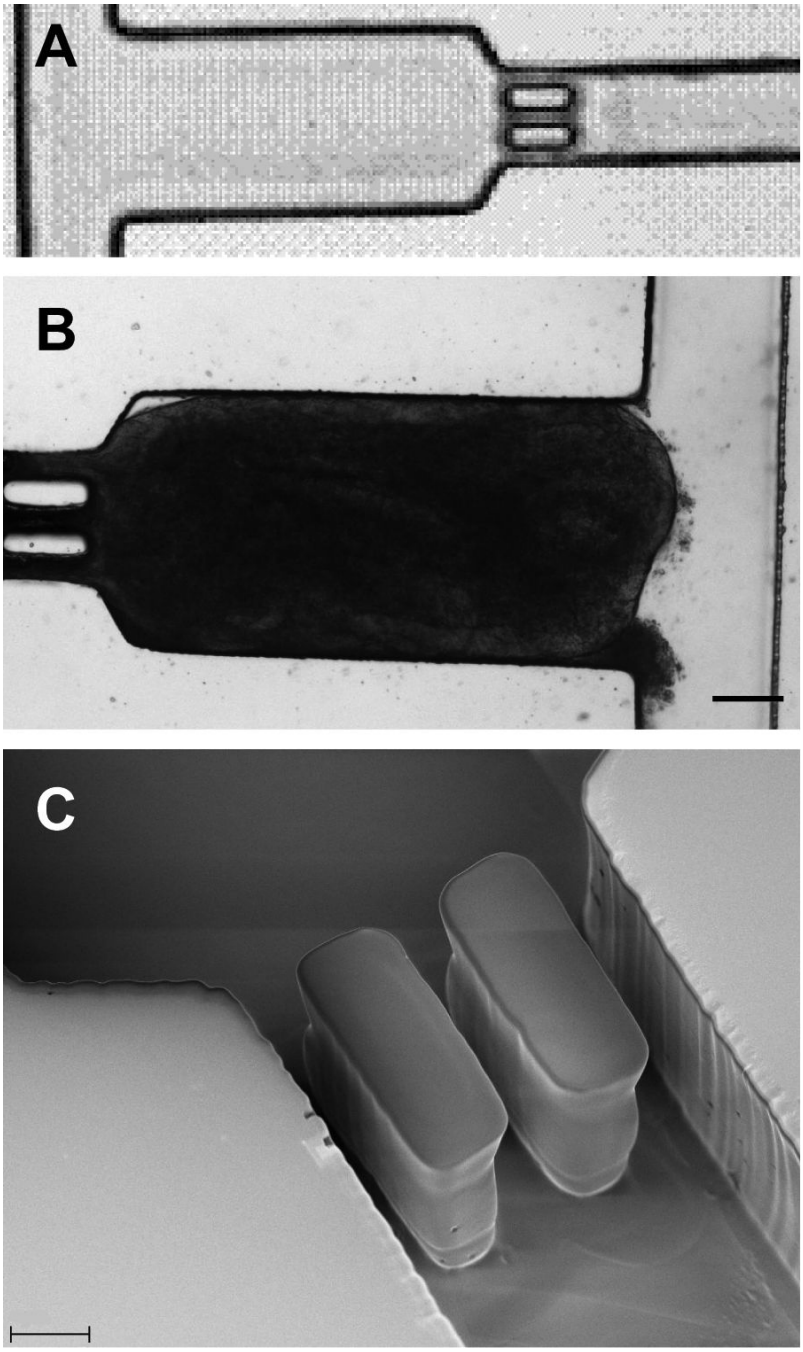

Figure 3. Tumor tissue chamber and cell-retention filter

A) Bright field image of the chamber and filter. Scale bar is 100 μm. *B)* Bright field image of tissue packed into the chamber. Scale bar is 100 μm. *C)* Scanning electron microscope image of the filter posts. Scale bar is 50 μm.

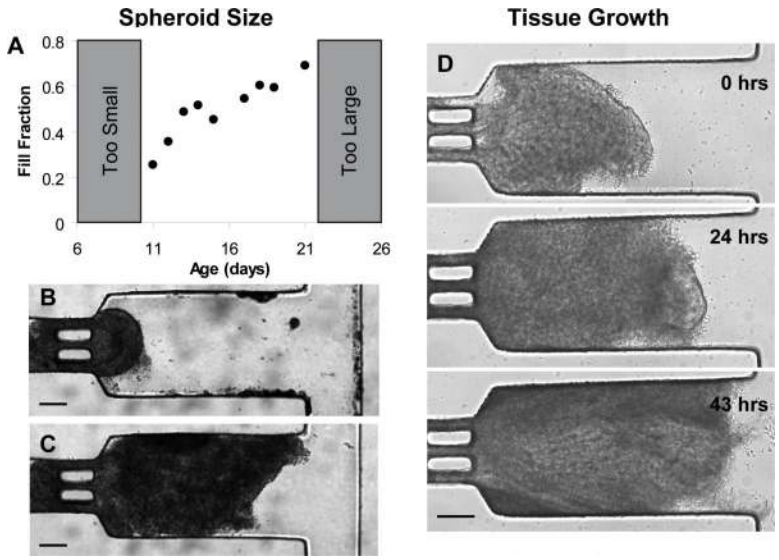

Figure 4. Effects of packed spheroid size and spheroid growth

A) Fill fraction increased as a function of the age of spheroid cultures prior to packing. Beneath 8 days old, spheroids were too small to be retained by the filter. Greater than 21 days old, spheroids were too fragile and broke apart during the packing process. *B)* Packed 11 day old spheroid. *C)* Packed 18 day old spheroid. D) Bright field images of tumor mass growing in the microfluidic device, acquired at 0, 24, and 43 hours. Scale bars are 100 μm.

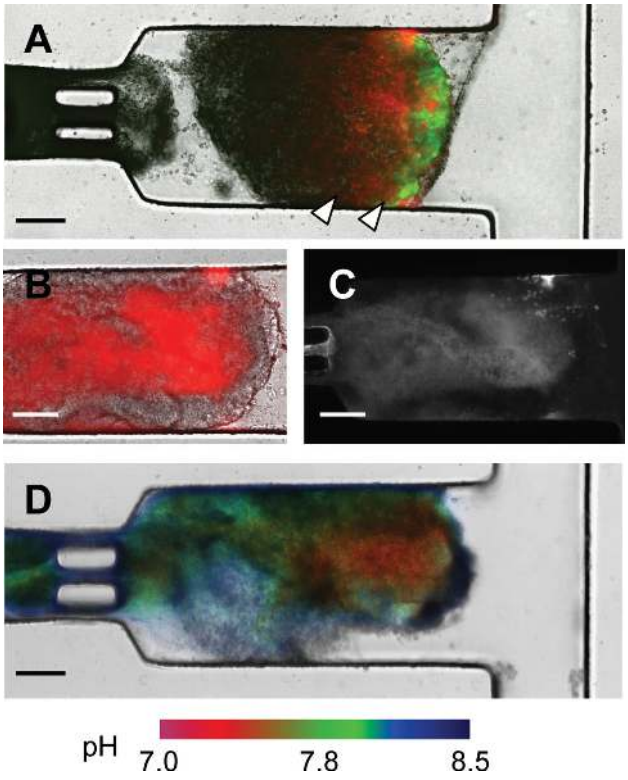

Figure 5. Microenvironment gradients in tumor tissue constrained by the device

A) Viability staining. Viable and dead cells are cells are stained green and red, respectively. Unstained cells at the distal end of the chamber were visibly necrotic in transmitted light images. White arrows indicate a region of newly formed dead cells bordering the edge of the chamber. *B, C)* Apoptosis staining. Cells indicated in red *(B)* and white *(C)* have active caspase-3, indicating commitment to programmed cell death. *D)* Cellular pH. Acidic and alkaline regions are indicated red and blue, respectively, and as designated by the scale. Scale bars are 100 μm.

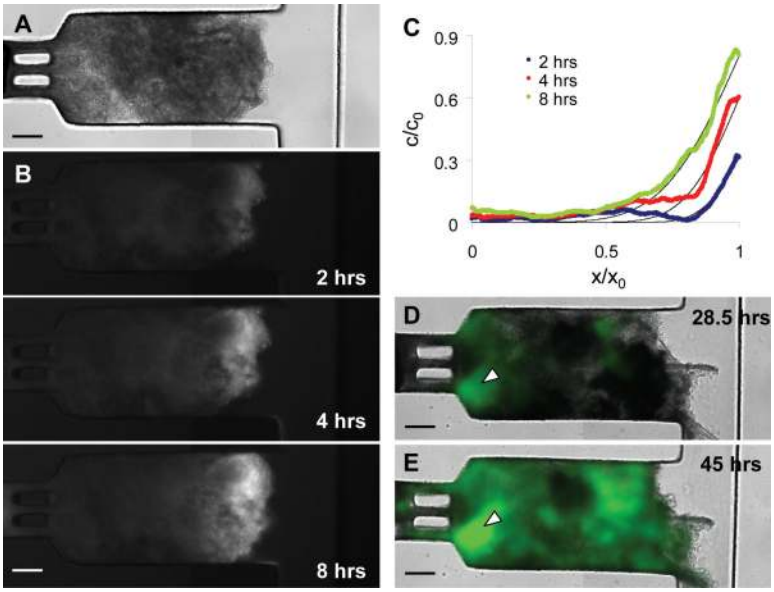

Figure 6. Diffusion and penetration of doxorubicin and therapeutic *Salmonella* bacteria

A) Bright field image of tissue used to measure drug diffusion, 24 hours after packing. *B)* Quantitative fluorescence images of doxorubicin diffusing into tumor tissue. *C)* Normalized concentration profiles derived from *(B)*. Model fits (black) were calculated using the average determined diffusion coefficient and closely fit experimental values. *D, E)* Bacterial accumulation in the device following inoculation with GFP-expressing *Salmonella typhimurium*. Images were acquired (*D*) at 28.5 after 20 hours of bacterial delivery and *(E*) at 45 hours after 16.5 hours of bacteria-free medium delivery. White arrows indicate a growing bacterial colony at the distal end of the chamber. Scale bars are 100 μm.